coatings

MDPI

Article

Nanomechanical Concepts in Magnetically Guided Systems to Investigate the Magnetic Dipole Effect on Ferromagnetic Flow Past a Vertical Cone Surface

Auwalu Hamisu Usman [1,2], Zahir Shah [3], Poom Kumam [4,5], Waris Khan [6] and Usa Wannasingha Humphries [1,*]

1 Department of Mathematics, Faculty of Science, King Mongkut's University of Technology Thonburi, 126 Pracha Uthit Road, Bang Mod, Thung Khru, Bangkok 10140, Thailand; auwalu.mth@mail.kmutt.ac.th
2 Department of Mathematical Sciences, Faculty of Physical Sciences, Bayero University, Kano 700241, Nigeria
3 Department of Mathematical Sciences, University of Lakki Marwat, Lakki Marwat 28420, Pakistan; zahir1987@yahoo.com
4 KMUTTFixed Point Research Laboratory, Room SCL 802 Fixed Point Laboratory, Department of Mathematics, Faculty of Science, King Mongkut's University of Technology Thonburi (KMUTT), Bangkok 10140, Thailand; poom.kum@kmutt.ac.th
5 Center of Excellence in Theoretical and Computational Science (TaCS-CoE), Faculty of Science, King Mongkut's University of Technology Thonburi (KMUTT), 126 Pracha-Uthit Road, Bang Mod, Thung Khru, Bangkok 10140, Thailand
6 Department of Mathematics and Statistics, Hazara University Mansehra, Khyber Pakhtunkhwa 21120, Pakistan; wariskhan758@yahoo.com
* Correspondence: usa.wan@kmutt.ac.th; Tel.: +66-024708831

Citation: Usman, A.H.; Shah, Z.; Kumam, P.; Khan, W.; Humphries, U.W. Nanomechanical Concepts in Magnetically Guided Systems to Investigate the Magnetic Dipole Effect on Ferromagnetic Flow Past a Vertical Cone Surface. *Coatings* **2021**, *11*, 1129. https://doi.org/10.3390/coatings11091129

Academic Editor: Eduardo Guzmán

Received: 16 August 2021
Accepted: 12 September 2021
Published: 16 September 2021

Abstract: Because of the floating magnetic nanomaterial, ferrofluids have magneto-viscous properties, enabling controllable temperature changes as well as nano-structured fluid characteristics. The study's purpose is to evolve and solve a theoretical model of bioconvection nanofluid flow with a magnetic dipole effect in the presence of Curie temperature and using the Forchheimer-extended Darcy law subjected to a vertical cone surface. The model also includes the nonlinear thermal radiation, heat suction/injection, viscous dissipation, and chemical reaction effects. The developed model problem is transformed into nonlinear ordinary differentials, which have been solved using the homotopy analysis technique. In this problem, the behavior of function profiles are graphically depicted and explained for a variety of key parameters. For a given set of parameters, tables representthe expected numerical values and behaviors of physical quantities. The nanofluid velocity decreases as the ferrohydrodynamic, local inertia, and porosity parameters increase and decrease when the bioconvection Rayleigh number increases. Many key parameters improved the thermal boundary layer and temperature. The concentration is low when the chemical reaction parameter and Schmidt number rises. Furthermore, as the bioconvection constant, Peclet and Lewis numbers rise, so does the density of motile microorganisms.

Keywords: ferromagnetic; nanofluid; bioconvection; porous medium; heat suction/injection; magnetic dipole

1. Introduction

Fluids that are often magnetized by the existence of an exterior magnetic field are known as ferrofluids, which is an abbreviation for fluid and ferromagnetic particles. These fluids are made up of colloidal fluids formed of nanosized ferromagnetic or ferrimagnetic particles that have been stopped inside the fluid transporter. Brownian motion causes particle suspension and must not start moving under normal conditions. Besides that, to avoid clogging, each ferromagnetic particle is encased in a solvent, and the nano-scaled ferromagnetic particles have a weak magnetic attraction whenever the surfactant's Van der Waals force adequately stopped aggregation or clustering. Numerous applications of ferromagnetic fluids have emerged in a variety of fields. Heat transfer agents, angular momentum changers, friction reducers, and so on are used in electronic equipment, analytical techniques, and medical science; some examples can be found in the references [1–3]. Because of these numerous applications, many researchers and scientists have been focused on this subject. Andersson and Vanes [4] first investigated the influence caused by magnetic dipoles on ferrofluids. Zeeshan et al. [5] investigated the convective heat transfer flow of ferromagnetic fluids with partial slip effects using a stretching sheet. Hayat et al. [6] reported on radiation and magnetic dipole effects of Williamson ferromagnetic fluid flow across a stretched surface.

A nanofluid is a nanometer-sized particle suspended in a fluid. Choi [7] established the basic extension of "nanofluid", and scientific results verified that heat transfer can be significantly enhanced through the mixture of tiny metallic nanomaterials with the working fluids. A few studies in particular on nanofluids have been conducted. Ellahi [8] performed an analytical study and concluded that the temperature variable and viscosity affects MHD non-Newtonian nanofluid flow in a pipe. Ellahi et al. [9] presented peristaltic nanofluid flow with entropy generation via a medium of porosity. Hayat et al. [10] investigated the flow of third-grade nanofluids caused by a rotating stretchable disk containing a heat source and a chemical reaction. Awais et al. [11] explored the effects of magnetohydrodynamics on peristaltic ciliary-induced flow coatings to rheological hybrid nanofluids. Reddy et al. [12] studied the boundary layer naturally convective MHD nanofluid flow along a vertical cone under the influence of chemical reaction and heat suction/injection.

Due to disorganized frameworks and destabilization, low-density microorganisms remain on the surface of a fluid, causing bioconvection. Because nanoparticles move differently than motile microorganisms, the cumulative importance of nanomaterials and bioconvection is such that they play a vital role in microfluidic devices. Bioconvection is a novel manufacturing and fluid mechanic with a biological phenomenon involving gyrotactic microorganisms. As a result, it becomes an interesting field of research to which many researchers continue to pay attention. Alsaedi et al. [13] investigated stratified magnetohydrodynamic nanofluid flow, causing bioconvection in gyrotactic microorganisms. Hayat et al. [14] researched the magnetohydrodynamic (MHD) nonlinear radiative nanofluid flow with gyrotactic microorganisms. Nadeem et al. [15] reported on the Rosseland assessment for ferromagnetic fluid with involvement of magnetic dipoles and gyrotactic microorganisms. Bhatti and Michaelides [16] researched thermo-bioconvection nanofluid flows across a Riga plate as a function of Arrhenius activation energy. Waqas et al. [17] have also numerically simulated the magnetized non-Newtonian bioconvection nanofluid flow along stretching cylinders/plates.

Combining mass and heat fluxes in liquid saturated porous media is crucial among a wide range of engineering procedures such as heating systems, oil and gas reservoirs, and chemical catalytic reactor designs [18,19]. The dragging force, the Darcy–Forchheimer technique, is a widely popular method for simulating fluid passed through a porous medium with high velocity. In the literature, flow through a cone in Darcy–Forchheimer porous media has already been analyzed by many researchers. Kumar et al. [20] investigated the non-Darcy MHD viscoelastic fluid flow through a flat plate and a vertical cone. Chamkha et al. [21] explored the non-Newtonian natural convective nanofluid flow over a saturated cone in a non-Darcy porous medium with uniform volume fraction and heat fluxes. Mallikarjuna et al. [22] researched the impacts of radiation, thermophoresis and transpiration on convective non-Darcy flow via a rotating cone. Durairaj et al. [23] investigated the chemically reacting Casson fluid of a non-Darcy porous medium flow through a flat plate and a vertical cone saturated with heat generating/absorbing. Patrulescu et al. [24] investigated a convection flow due to a vertical plate embedded in a bi-disperse non-Darcy porous medium.

According to a recent literature review, despite important applications in extrusion systems, geothermics, organic compounds, geophysics, improved manufacturing techniques, material processing, and improved energy generation, research on viscous ferrofluid flows via a linear vertical cone with consideration of Darcy–Forchheimer porous media has been studied by very few researchers in the past. The aim of this research is to use the Forchheimer-extended Darcy law to explore the effect of magnetic dipole and porosity relations in the boundary layer of a ferromagnetic nanofluid flow via a vertical cone surface. The study of the effect of the magnetic dipole on ferromagnetic nanofluid flow via the vertical cone surface makes this work different from the existing literature. A nonlinear ordinary differential equation replaces the governing equations and is solved using HAM techniques. Initially, Liao [25–27] presented a homotopy analysis method with HAM. The method has fast convergent solutions with many advantages over some existing methods. Various researchers have been drawn to it as a result of its rapid convergence [28–31]. The results collected for all associated parameters on all profiles are shown graphically. The validation of the results by comparing them to previously published material in the literature is an important feature of the presented model. In this regard, illustrious coherence has been attained.

2. Materials and Methods

An incompressible electrically conducting viscous nanofluid flow via a vertical cone with bioconvection is explored in two dimensions as an axisymmetric, steady, natural convective ferrofluid flow. Furthermore, it is postulated that temperature and concentration are non-uniform at the surface due to the influence of heat generation/absorption, chemical reaction and viscous dissipation. The flow is electrically magnetized by a magnetic dipole, and a Darcy–Forchheimer porous medium model is also used. Thermal radiation exists as a unidirectional flux in the transverse to the cone surface (s-direction). In comparison to the s-direction, the radiation heat flux in the x-direction is considered neglected. The x-axis of the chosen coordinate system corresponds to the direction of flow over the cone surface. T_w is taken to be the temperature at the cone's surface ($s = 0$), and the concentration is governed by the condition $D_B \frac{\partial C}{\partial s} + \frac{D_T}{T_\infty}\frac{\partial T}{\partial s} = 0$ at the cone's surface, where T_∞ is the temperature and C_∞ is the concentration and N_∞ density of microorganisms in the ambient nanofluid.

The boundary layer equation [12,14,21] based on the assumptions stated above are the equations of continuity and momentum as well as energy, concentration, and microorganisms:

$$\frac{\partial(ru)}{\partial x} + \frac{\partial\{(rw)\}}{\partial s} = 0, \tag{1}$$

$$\begin{aligned} w\frac{\partial u}{\partial s} + u\frac{\partial u}{\partial x} = \frac{\mu_f}{\rho_f}\frac{\partial^2 u}{\partial s^2} - \frac{\mu_f}{k_o^*}u - \frac{\rho_f C_b}{\sqrt{k_o^*}}u^2 + \lambda_o M\frac{\partial H}{\partial x} \\ + g\Big[\beta_T(T - T_\infty) + \beta_C(C - C_\infty) + \beta_N(N - N_\infty)\Big]cos(\alpha), \end{aligned} \tag{2}$$

$$\begin{aligned} w\frac{\partial T}{\partial s} + u\frac{\partial T}{\partial x} = \alpha_f\frac{\partial^2 T}{\partial s^2} + \frac{\mu_f}{(\rho c_p)_f}\left(\frac{\partial u}{\partial s}\right)^2 + \left(u\frac{\partial H}{\partial x} + w\frac{\partial H}{\partial s}\right)\frac{\lambda_0}{(\rho c_p)_f}T\frac{\partial M}{\partial T} \\ \tau\left[D_B\frac{\partial C}{\partial s}\frac{\partial T}{\partial s} + \frac{D_T}{T_\infty}\left(\frac{\partial T}{\partial s}\right)^2\right] - \frac{1}{(\rho c_p)_f}\frac{\partial q_r}{\partial s}, \end{aligned} \tag{3}$$

$$w\frac{\partial C}{\partial s} + u\frac{\partial C}{\partial x} = D_B\frac{\partial^2 C}{\partial s^2} + \frac{D_T}{T_\infty}\frac{\partial^2 T}{\partial s^2} - K_r(C - C_\infty), \tag{4}$$

$$w\frac{\partial N}{\partial s} + u\frac{\partial N}{\partial x} + \frac{bW_c}{C_w - C_\infty}\left(\frac{\partial C}{\partial s}\frac{\partial N}{\partial s} + N\frac{\partial^2 C}{\partial s^2}\right) = D_n\frac{\partial^2 N}{\partial s^2}, \tag{5}$$

with initial boundary conditions

$$u = 0, \ \ w = W_w, \ T = T_w, \ -D_B \frac{\partial C}{\partial s} = \frac{D_T}{T_\infty} \frac{\partial T}{\partial s}, \ N = N_w \ at \quad s = 0, \tag{6}$$

$$u \to 0, \quad w \to 0, \quad T \to T_\infty, \ \ C \to C_\infty, \quad N \to N_\infty, \quad as \quad s \to \infty, \tag{7}$$

where (u,w) are the velocity components in the x-direction (radial) and s-direction (transverse), respectively; T, C, N are the temperature, concentration, and gyrotactic microorganism, respectively; the diffusion coefficients named Brownian, thermophoresis, and microorganism correspond to D_B, D_T, and D_n, respectively; while τ is the ratio of heat capacitance, fluid density is ρ_f, thermal conductivity of fluid is k_f , electrical conductivity of fluid is σ , the dynamic viscosity is μ_f, thermal diffusivity of base fluid is α_f, magnetic permeability is λ_o, heat capacitance of fluid is $(\rho c_p)_f$, first order chemical reaction parameter is K_r, speed of gyrotactic cell is W_c, and b is chemotaxis.

Magnetic Dipole

The magnetic field features impacted the ferrofluid flow with magnetic dipole effects detected mostly by magnetic scalar potential Φ_1, as given in Equation (8):

$$\Phi_1 = \frac{\gamma}{2\pi} \frac{x}{x^2 + (s+c)^2}, \tag{8}$$

Considering H_x and H_s to be the components of magnetic field, with γ as the magnetic field strength at the source, see Equations (9) and (10):

$$H_x = -\frac{\partial \Phi_1}{\partial x} = \frac{\gamma}{2\pi} \frac{x^2 - (s+d)^2}{[x^2 + (s+d)^2]^2} \tag{9}$$

$$H_s = -\frac{\partial \Phi_1}{\partial s} = \frac{\gamma}{2\pi} \frac{2x(s+d)}{[x^2 + (s+d)^2]^2}. \tag{10}$$

As the strength of a magnetic body is normally approximately equal to the H_x and H_s gradients, it is therefore given as in (11):

$$H = \sqrt{H_x^2 + H_s^2}. \tag{11}$$

Equation (12) displays the approximate linearized relation of the magnetization M as function of temperature T,

$$M = -K_1(T_\infty - T), \tag{12}$$

with K_1 identified as the ferromagnetic coefficient. Figure 1 depicts the physical configuration of the heated ferrofluid.

Considering the following transformations, given the stream function as $\Phi(x,s)$, such that

$$u = \frac{1}{r} \frac{\partial \Phi}{\partial s} \qquad\qquad w = -\frac{1}{r} \frac{\partial \Phi}{\partial x} \tag{13}$$

with $\Phi(x,s) = \nu_f r Ra_x f(\zeta)$ and Ra_x is the Rayleigh number given by $Ra_x = \frac{\rho_f \beta_T g (T_w - T_\infty) x^3 cos(\alpha)}{\nu_f^2}$, therefore, the following are given:

$$u = \frac{\nu_f Ra_x^{\frac{1}{2}}}{x} f'(\zeta), \ \ w = -\frac{\nu_f Ra_x^{\frac{1}{4}}}{x} \Big(\zeta f'(\zeta) - f(\zeta) \Big), \ \ \zeta = \frac{s}{x} Ra_x^{\frac{1}{4}},$$
$$(T_w - T_\infty)\theta(\zeta) = (T - T_\infty), \ \ (C_w - C_\infty)\phi(\zeta) = (C - C_\infty), \ \ (N_w - N_\infty)\chi(\zeta) = (N - N_\infty). \tag{14}$$

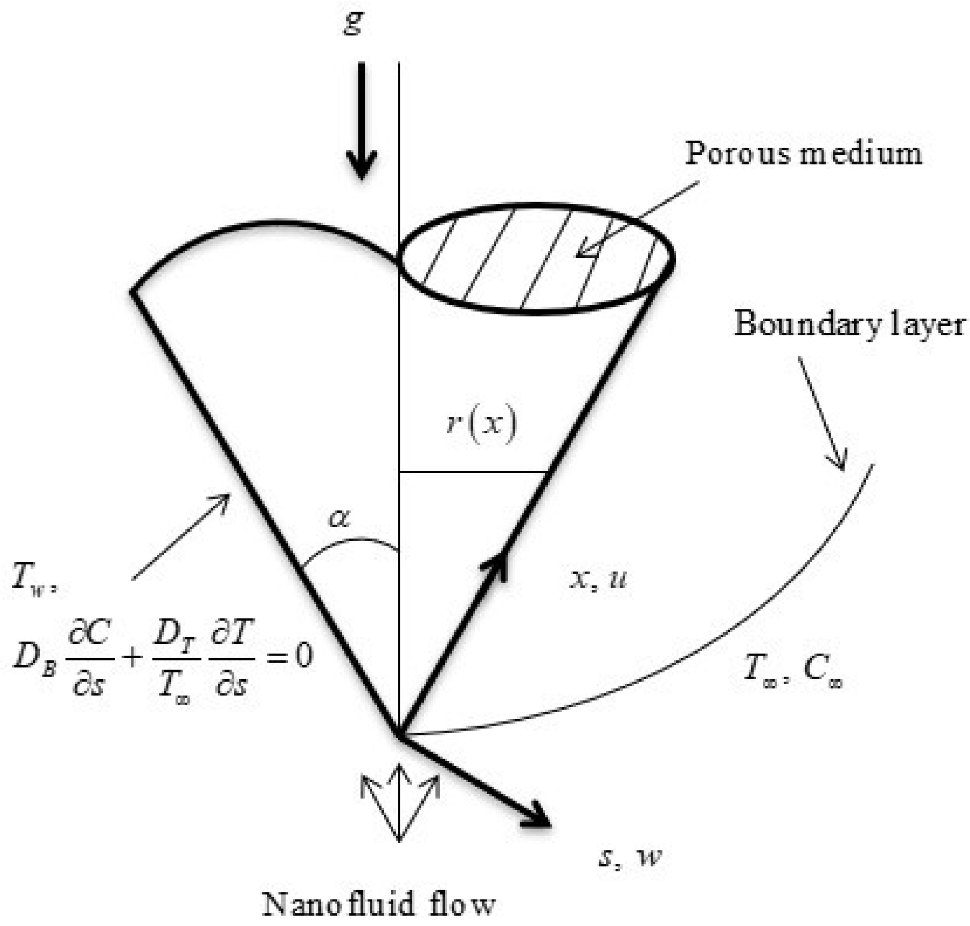

Figure 1. A picture scheme of the problem.

Taking r to be approximately the cone local radius, for the thermal boundary layer becoming thin, it will be along the x coordinate with $r = xsin(\alpha)$.

By using the above transformations, Equation (1) will be satisfactory, and Equations (2)–(5) will be

$$f''' - P_1 f' + ff'' - F_r f'^2 + \frac{2\beta}{(\zeta+\alpha_1)^4}(1+\theta) + N_c\phi + Ra_b\chi = 0, \tag{15}$$

$$\begin{aligned}(1+Rd)\theta'' + Prf\theta' + Nb\phi'\theta' + Nt(\theta')^2 + \frac{2Pr\beta\lambda(\theta-\epsilon)(f-\zeta f')}{(\zeta+d\alpha_1)^3} \\ + Pr\beta\lambda(\theta-\epsilon)\left[\frac{2f'}{(\zeta+\alpha_1)^4} + \frac{4(\zeta f'-f)}{(\zeta+\alpha_1)^5}\right] + PrEc(f'')^2 = 0,\end{aligned} \tag{16}$$

$$\phi'' + \frac{Nt}{Nb}\theta'' + Scf\phi' - \delta Sc\phi = 0, \tag{17}$$

$$\chi'' - Pe[\phi'\chi' + \phi''\chi + \delta_n\phi''] + Lbf\chi' = 0. \tag{18}$$

Moreover, with the new boundary conditions:

$$\begin{aligned}&f' = 1, f = S, \theta = 1, Nb\phi' + Nt\theta = 0, \chi = 1 at \zeta = 0,\\ &f' \to 0, \theta \to 0, \phi \to 0, \chi \to 0, as \zeta \to \infty,\end{aligned} \tag{19}$$

where α_1 is dimensionless distance, N_c is the ratio due to buoyancy force, Ra_b is the bioconvection Rayleigh number, β is the ferrohydrodynamic interaction parameter, ε the Curie temperature, λ is the heat dissipation parameter, S is the heat generation/absorption parameter ($S > 0$ for suction and $S < 0$ for injection), Nb and Nt are the Brownian motion and thermophoresis parameters, the Prandtl number is Pr, the Eckert number is Ec, the radiation parameter is Rd, the local inertia parameter is F_r, the chemical reaction parameter is δ, the porosity parameter is P_1, the Schmidt number is Sc, the Lewis number of bioconvection is Lb, the Peclet number Pe, δ_n is the bioconvection constant, and quantities are defined by

$$\begin{aligned}
&S = \frac{W_w x}{\nu_f Ra^{\frac{1}{2}}}, N_c = \frac{g\beta_C(C_w - C_\infty)x^3 cos(\alpha_1)}{\nu_f^2 Ra_x}, Ra_b = \frac{g\beta_N(N_w - N_\infty)x^3 cos(\alpha)}{\nu_f^2 Ra_x}, P_1 = \frac{\mu_f}{k_o^*},\\
&L_i = \frac{C_b}{\sqrt{k_o^*}}, \beta = \frac{\gamma\lambda_o K\rho_f(T_w - T_\infty)}{2\pi\mu_f^2}, Pr = \frac{\mu_f c_p}{k_f}, Ec = \frac{W_w^2}{c_p(T_w - T_\infty)}, \lambda = \frac{\mu_f^2}{\rho_f(T_w - T_\infty)Ra_x^{\frac{3}{4}}},\\
&\delta = \frac{K_1 x^2}{\nu_f Ra_x^{\frac{1}{2}}}, Rd = \frac{16\sigma^* T_\infty^3}{3k^* k_f}, Sc = \frac{\nu_f}{D_B}, Pe = \frac{bW_c}{D_n}, Lb = \frac{\nu_f}{D_n}, \epsilon = \frac{T_\infty}{T_\infty - T_w},\\
&d = \frac{aRa_x}{x}, Nt = \frac{\tau D_T(T_w - T_\infty)}{T_\infty \alpha_f}, Nb = \frac{\tau D_B(C_w - C_\infty)}{\alpha_f}, \delta_n = \frac{N_\infty}{N_w - N_\infty}.
\end{aligned} \tag{20}$$

The local Nusselt, Sherwood, and local Density expressions, as well as the coefficient of skin friction, will be computed by

$$C_f = \frac{2\tau_w}{\rho_f W_w^2}, Nu_x = \frac{q_h x}{k_f(T_w - T_\infty)}, Sh_x = \frac{q_m x}{D_B(C_w - C_\infty)}, Sn_x = \frac{q_n x}{D_n(N_w - N_\infty)}, \tag{21}$$

$$\tau_w = \mu_f u_s|_{s=0}, q_h = [-k_f T_s + q_r]|_{s=0}, q_m = -D_B C_s|_{s=0}, q_n = -D_n N_s|_{s=0}, \tag{22}$$

$$Ra_x^{\frac{1}{4}} C_f = 2f''(0), Nu = -Ra_x^{\frac{1}{4}}(1 + Rd)\theta'(0), Sh = -Ra_x^{\frac{1}{4}}\phi'(0), Sn = -Ra_x^{\frac{1}{4}}\chi'(0). \tag{23}$$

3. HAM Solutions Methodology

The homotopy analysis method (HAM) was applied to solve Equations (15)–(18). Shijun Liao developed this technique in 1992. It is often valid, regardless of whether there are a limited number of parameters or otherwise. It can be used to solve both weakly and strongly nonlinear problems. It offers a wide range of options for selecting the base functions of solutions, as well as discretion in choosing the linear operators. However, it provides a convenient method for ensuring the convergence of series solutions. Therefore, this method differs from other techniques, with examples like Adomain decomposition and the delta expansion methods. In the introduction section, some studies on the approach were presented.

Taking the initial guesses of the $f(\zeta)$,$\theta(\zeta)$, $\phi(\zeta)$, and $\chi(\zeta)$ with the auxiliary linear operators respectively as

$$f_0(\zeta) = 1 - e^{-\zeta},\ \theta_0(\zeta) = \left(\frac{B_i}{1 + B_i}\right)e^{-\zeta},\ \phi_0(\zeta) = -\left(\frac{Nt}{Nb}\right)e^{-\zeta},\ \chi_0(\zeta) = e^{-\zeta}. \tag{24}$$

and

$$\mathcal{L}_f = f''' - f',\ \ \mathcal{L}_\theta = \theta'' - \theta,\ \ \mathcal{L}_\phi = \phi'' - \phi,\ \ \mathcal{L}_\chi = \chi'' - \chi, \tag{25}$$

the properties are satisfied as given below

$$
\begin{aligned}
&\mathcal{L}_f(\Lambda_1 + \Lambda_2 e^{\zeta} + \Lambda_3 e^{-\zeta}) = 0, \;\; \mathcal{L}_\theta(\Lambda_4 e^{\zeta} + \Lambda_5 e^{-\zeta}) = 0, \\
&\mathcal{L}_\phi(\Lambda_6 e^{\zeta} + \Lambda_7 e^{-\zeta}) = 0, \;\; L_\chi(\Lambda_8 e^{\zeta} + \Lambda_9 e^{-\zeta}) = 0
\end{aligned} \tag{26}
$$

with arbitrary constants $\Lambda_i, i \in [1,9]$. The Zeroth order form of the problem is given by

$$(1-p)\mathcal{L}_f[f(\zeta;p) - f_0(\zeta)] = ph_f \mathbf{N}_f[f(\zeta,p), \theta(\zeta,p), \phi(\zeta,p), \chi(\zeta,p)], \tag{27}$$

$$(1-p)\mathcal{L}_\theta[\theta(\zeta;p) - \theta_0(\zeta)] = ph_\theta \mathbf{N}_\theta[\theta(\zeta,p), f(\zeta,p), \phi(\zeta,p)], \tag{28}$$

$$(1-p)\mathcal{L}_\phi[\phi(\zeta,p) - \phi_0(\zeta)] = ph_\phi \mathbf{N}_\phi[\phi(\zeta,p), \theta(\zeta,p), f(\zeta,p)], \tag{29}$$

$$(1-p)\mathcal{L}_\chi[\chi(\zeta,p) - \chi_0(\zeta)] = ph_\chi \mathbf{N}_\chi[\chi(\zeta,pp), \phi(\zeta,p), f(\zeta,p)], \tag{30}$$

with $p \in [0,1]$ as the embedded parameter, and nonlinear operators $\mathbf{N}_f$, $\mathbf{N}_\theta$, $\mathbf{N}_\phi$, and $\mathbf{N}_\chi$ obtained by using Equations (15)–(18).

The problems' equivalent m order of the deformation are

$$L_f[f_m(\zeta,p) - \eta_m f_{m-1}(\zeta)] = h_f \mathcal{R}_{f,m}(\zeta), \tag{31}$$

$$\mathcal{L}_\theta[\theta_m(\zeta,p) - \eta_m \theta_{m-1}(\zeta)] = h_\theta \mathcal{R}_{\theta,m}(\zeta), \tag{32}$$

$$\mathcal{L}_\phi[\phi_m(\zeta,p) - \eta_m \phi_{m-1}(\zeta)] = h_\phi \mathcal{R}_{\phi,m}(\zeta), \tag{33}$$

$$\mathcal{L}_\chi[\chi_m(\zeta,p) - \eta_m \chi_{m-1}(\zeta)] = h_\chi \mathcal{R}_{\chi,m}(\zeta), \tag{34}$$

$$
\begin{aligned}
&f_m = S, f'_m = 0, \theta'_m - B_i\theta_m = 0, Nb\phi'_m + Nt\theta'_m = 0, \chi_m = 0, at\ \zeta = 0 \\
&f'_m = 0, \theta_m = 0, \phi_m = 0, \chi_m = 0 as \zeta \to \infty.
\end{aligned} \tag{35}
$$

$$\eta_m = \begin{cases} 0, & \text{if } m \le 1 \\ 1, & \text{if } m > 1, \end{cases} \tag{36}$$

where $\mathcal{R}_f^m(\zeta)$,$\mathcal{R}_\theta^m(\zeta)$,$\mathcal{R}_\phi^m(\zeta)$,$\mathcal{R}_\chi^m(\zeta)$ can be obtained using Equations (15)–(18).

The general solutions are given by

$$f_m(\zeta) = f_m^s(\zeta) + \Lambda_1 + \Lambda_2 e^{\zeta} + \Lambda_3 e^{-\zeta}, \tag{37}$$

$$\theta_m(\zeta) = \theta_m^s(\zeta) + \Lambda_4 e^{\zeta} + \Lambda_5 e^{-\zeta}, \tag{38}$$

$$\phi_m(\zeta) = \phi_m^s(\zeta) + \Lambda_6 e^{\zeta} + \Lambda_7 e^{-\zeta}, \tag{39}$$

$$\chi_m(\zeta) = \chi_m^s(\zeta) + \Lambda_8 e^{\zeta} + \Lambda_9 e^{-\zeta}, \tag{40}$$

where $(f_m^s(\zeta), \theta_m^s(\zeta), \phi_m^s(\zeta), \chi_m^s(\zeta))$ are special solutions.

4. Analysis of Convergence of the Solutions

The convergence Table 1 is organized for each profile up towards the 35th order of approximation. Table 2 compares the current work to the published work and reveals that there is very close agreement.

Table 1. Convergence of HAM solutions with order approximations.

Order of Approximations	$-f''(0)$	$-\theta'(0)$	$-\phi'(0)$	$-\chi'(0)$
1	1.87633	0.6333	1.12222	0.69596
5	1.93521	0.76748	1.12327	0.69583
10	1.93385	0.76804	1.12349	0.69575
15	1.93135	0.7658	1.12354	0.69575
25	1.93026	0.7658	1.12354	0.69575
30	1.93026	0.7658	1.12354	0.69575
35	1.93026	0.7658	1.12354	0.69575

Table 2. Comparison of $-\theta'(0)$ and $-\phi'(0)$ by alternating buoyancy ratio parameter N_c with published work.

N_c	$-\theta'(0)$ Reddy et al. [12]	Present	$-\phi'(0)$ Reddy et al. [12]	Present
0.1	0.32598	0.32601	1.48394	1.48381
0.2	0.32405	0.32411	1.46789	1.46801
0.3	0.32229	0.32231	1.45214	1.45215
0.4	0.32125	0.32129	1.43598	1.43594
0.5	0.31868	0.31867	1.41938	1.41940

5. Results and Discussion

The role of β on velocity profile is detected in Figure 2. The ferromagnetic parameter emphasizes the effect of the magnetic dipole's external magnetic field on fluid dynamics. As the magnetic field acts as a deforming force, the axial velocity decreases. Figure 3 depicts the important properties of the Fr on the dimensionless velocity. Obviously, increasing Fr causes the velocity of fluid layers to decrease. From a physical standpoint, the local inertia parameter generates resistance forces against the motion of fluid particles. Moreover, as the local inertia parameter increases, so does the velocity. Figure 4 depicts the impact of increasing P_1 on the velocity. The porosity parameter is defined as the kinematic viscosity to permeability strength of porous space ratio. As the porosity parameter increases, the velocity curves definitely decrease. Figure 5 depicts the effect of the Ra_b on the velocity profile. It was discovered that when the values of Ra_b rise, the velocity accelerates. As a result of the buoyancy forces caused by bioconvection, the fluid velocity increases by increasing the bioconvection Raleigh number. Figure 6 shows that the temperature on the boundary layers enhances as a result of increasing the values of β. This is due to an interaction of the fluid's movement and the interference of the ferromagnetic particles. The interplay reduces the velocity while frictional heating increases between the fluid layers, resulting in an increase in the thermal boundary layer thickness. The effect of λ on the temperature profile is depicted in Figure 7. In this case, temperature is displayed as an increasing function of λ. Usually, as the values of λ increase, so does the thermal conductivity, and thus the temperature. Figure 8 displays the role of Fr on temperature profile. A rise in Fr results in a rise in temperature and the thermal boundary layer thickness. Figure 9 reveals that as B_i increases, so does the thickness of the thermal boundary layer, and the temperature also enhances. A higher Biot number contributes to more convection, which leads to the enhancement of the temperature and thermal boundary layer thickness. Figure 10 shows the effect of $S < 0$ on the dimensionless temperature. This figure reveals that when increasing $S < 0$, the temperature and the thickness of the thermal boundary layers both decrease. As an outcome, suction is removed from the warm fluid in the boundary layer region to a large extent. Moreover, the opposite trend is observed in the temperature profile, as shown in Figure 11 with $S > 0$. This is attributable to the fact that the temperature of the fluid is raised by injecting warm fluid into the boundary layer region. Figure 12 depicts the effects of Rd on the temperature profile for various Rd values.

An increase in the Rd causes a rise in the temperature, and the effect of thermal radiation improves the medium's thermal diffusive. Besides that, for higher Nt values, temperatures rise in the boundary layer region (Figure 13). The thermophoretic force developed in the boundary layer regime is an outcome of the temperature gradient; such forces entail the diffusion of nanoparticles out of the higher temperature area to a lower temperature area, leading to a thermal boundary layer thickness enhancement. Figure 14 depicts the Nb characteristics on a temperature profile. Usually, a rise in Nb improves the motion of fluid particles randomly, resulting in more heat generation. As a result, the temperature rises. Figure 15 depicts the temperature distribution by raising Ec values. The Ec defines the connection among the flow of kinetic energy and heat enthalpy variation. As a consequence, raising Ec also raises the kinetic energy. Moreover, temperature is well understood to be defined as average kinetic energy. As a result, the fluid's temperature rises. This graph shows that as Ec increases, so does the temperature. Figure 16 shows the role of Pr on the temperature profile. It has been discovered that raising the Pr lowers the temperature of the fluid flow. Large Pr values clearly result in the thinning of thermal boundary layers. As δ increases, so does the concentration profile. The concentration becomes less effective as the delta values increase, as shown in Figure 17. The physical effect of Nb on a concentration profile is depicted in Figure 18. Brownian motion does play a role in determining the efficiency of heat transfer during nanofluid flow. The nanoparticles collide with one another and transfer energy due to the random motion of a nanofluid. As a result, as Nb levels rise, the concentration profile falls. The effect of Nt on nanoparticle concentration is depicted in Figure 19. The concentration field rises in this case due to an increase in Nt. Larger Nt causes an increase in thermophoresis forces, which further frequently carries nanomaterials from higher to lower temperature regions. As a result, the concentration decreases. The effect of Sc on concentration is depicted in Figure 20. Sc denotes the momentum-to-mass diffusivity ratio, which measures the relative efficacy of momentum and mass transport through diffusion within concentration boundary layers. Figures 21 and 22 show the effects of Pe and Lb on the microorganism profile. According to these figures, the microorganism field decreases with increase of both numbers. According to Table 3, as Pr estimates increase, so does the Nusselt number. Table 4 shows that as δ and Sc increase, so does the Sherwood number. The results of motile microorganism density are increased by increasing Lb and Ra_b, as shown in Table 5.

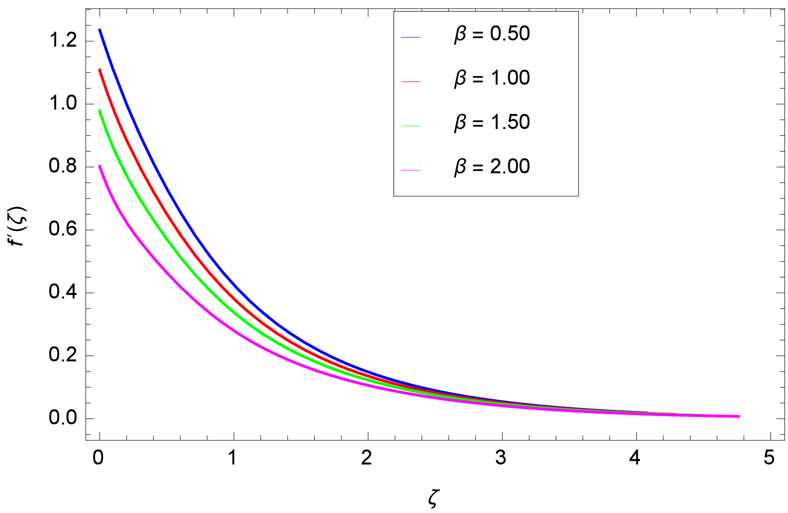

Figure 2. Influence of β on $f'(\zeta)$.

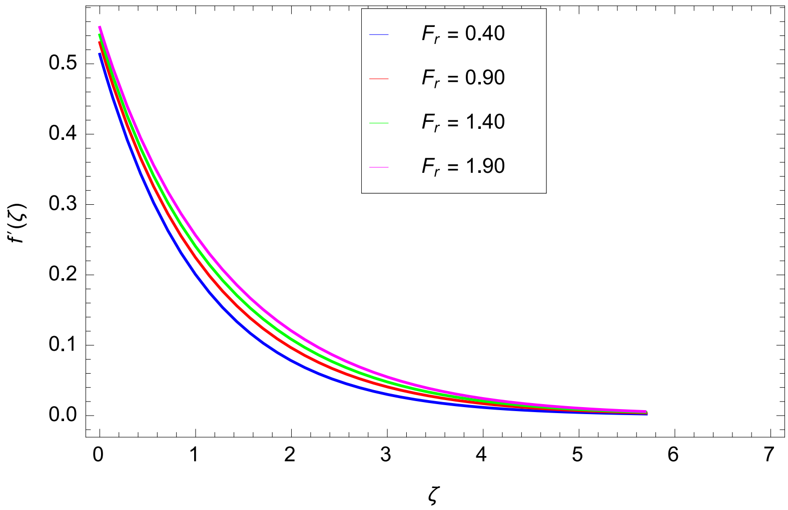

Figure 3. Influence of Fr on $f'(\zeta)$.

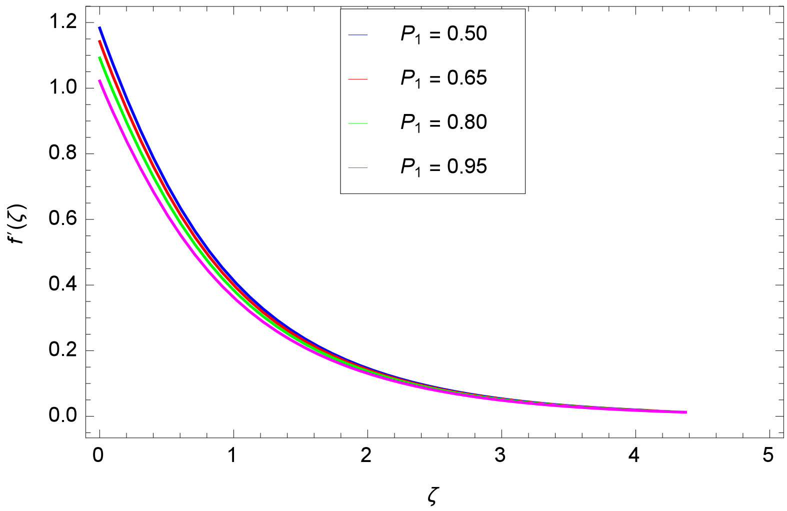

Figure 4. Influence of P_1 on $f'(\zeta)$.

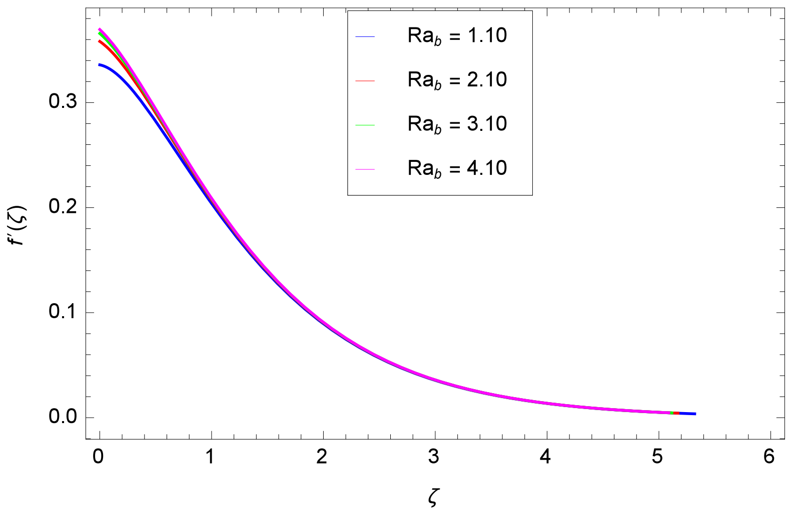

Figure 5. Influence of Ra_b on $f'(\zeta)$.

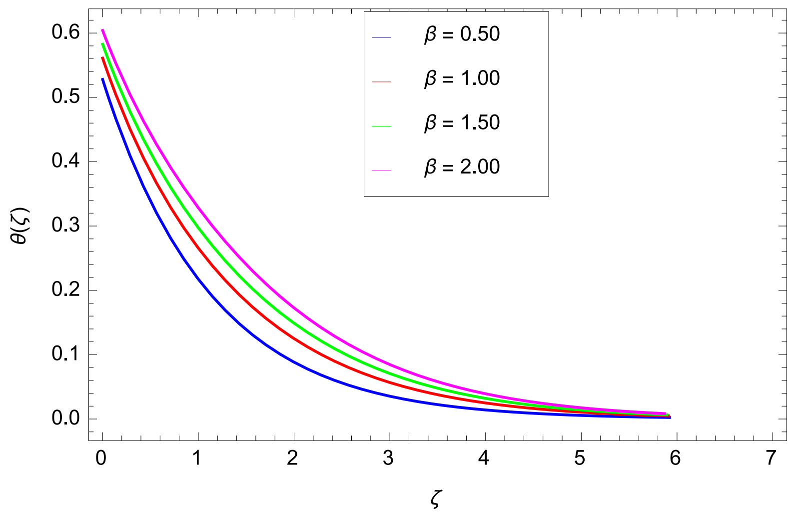

Figure 6. Influence of β on $\theta(\zeta)$.

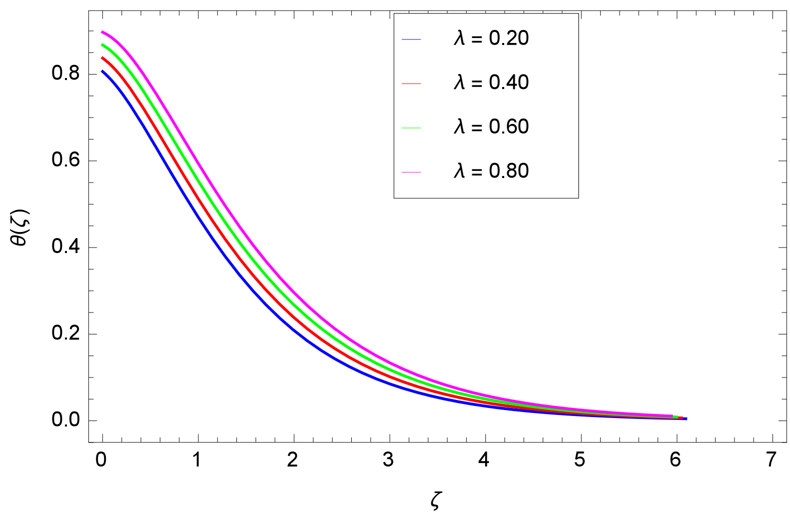

Figure 7. Influence of λ on $\theta(\zeta)$.

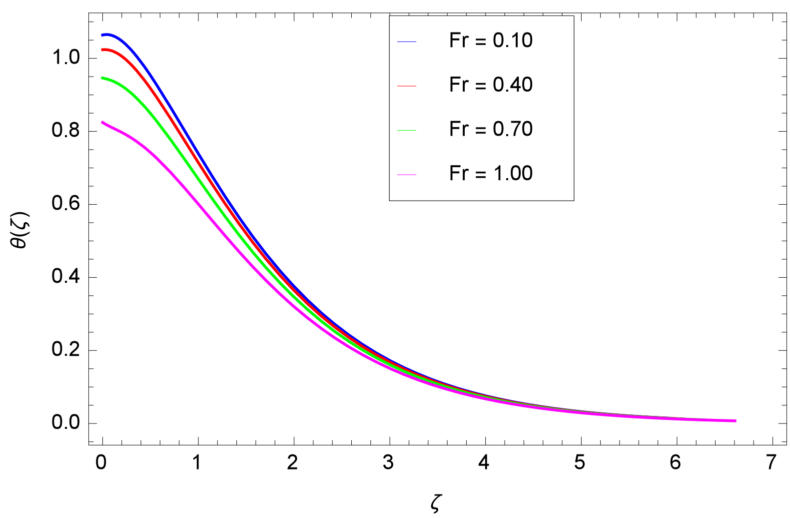

Figure 8. Influence of Fr on $\theta(\zeta)$.

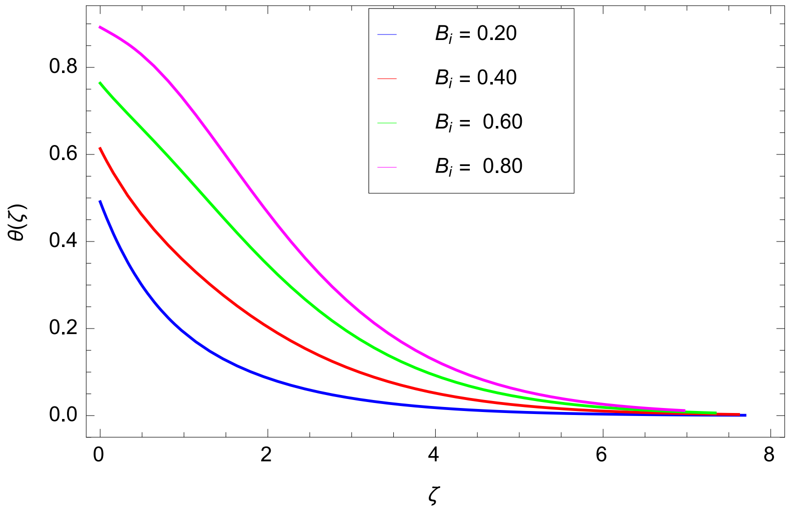

Figure 9. Influence of B_i on $\theta(\zeta)$.

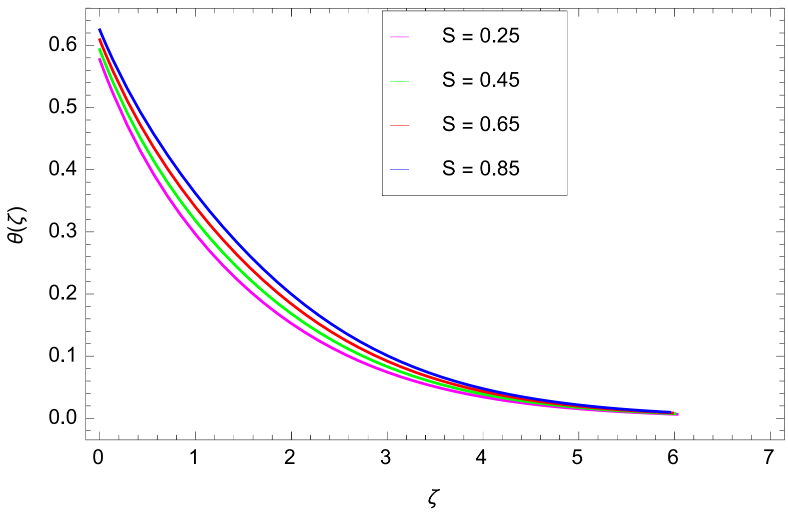

Figure 10. Influence of $S < 0$ on $\theta(\zeta)$.

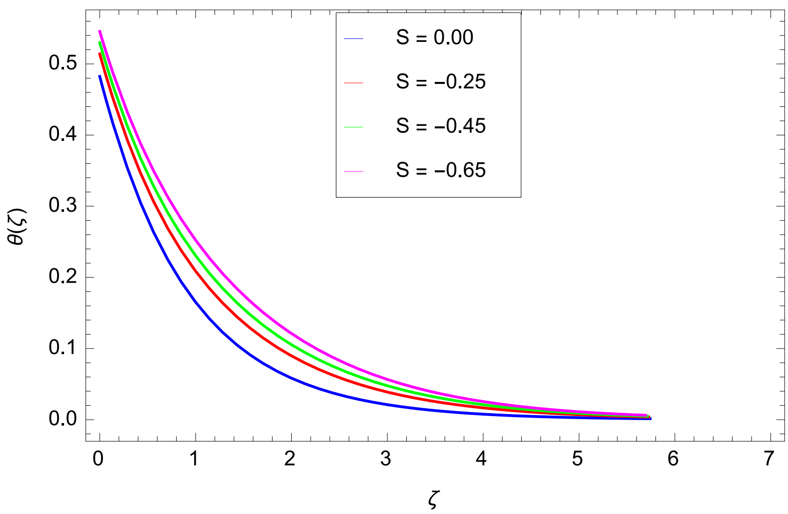

Figure 11. Influence of $S > 0$ on $\theta(\zeta)$.

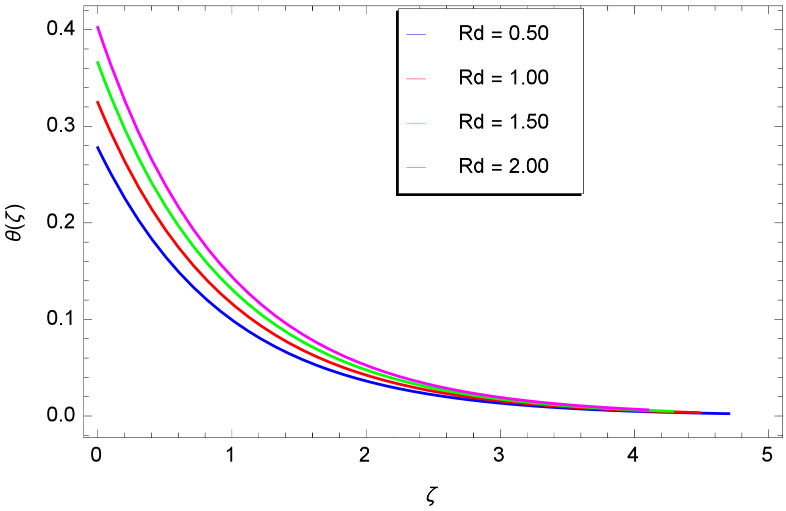

Figure 12. Influence of Rd on $\theta(\zeta)$.

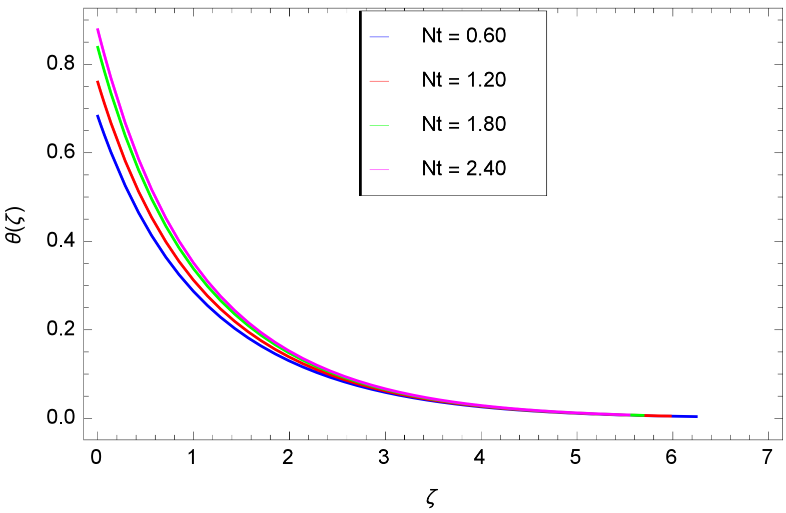

Figure 13. Influence of Nt on $\theta(\zeta)$.

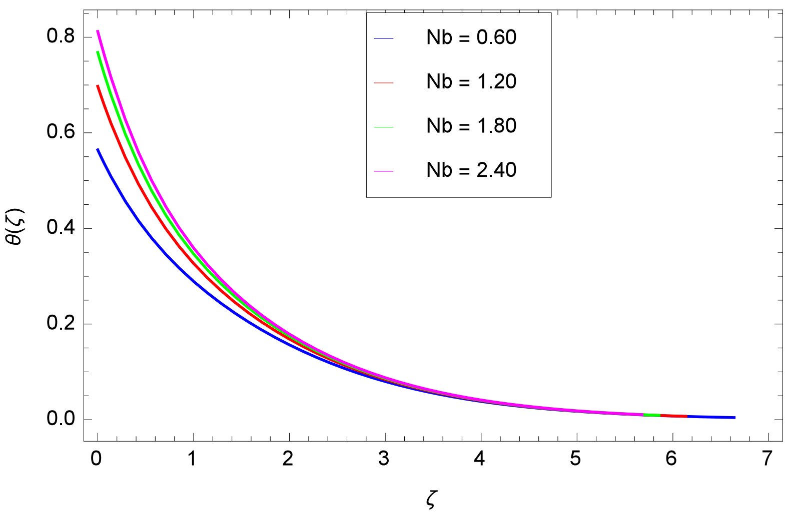

Figure 14. Influence of Nb on $\theta(\zeta)$.

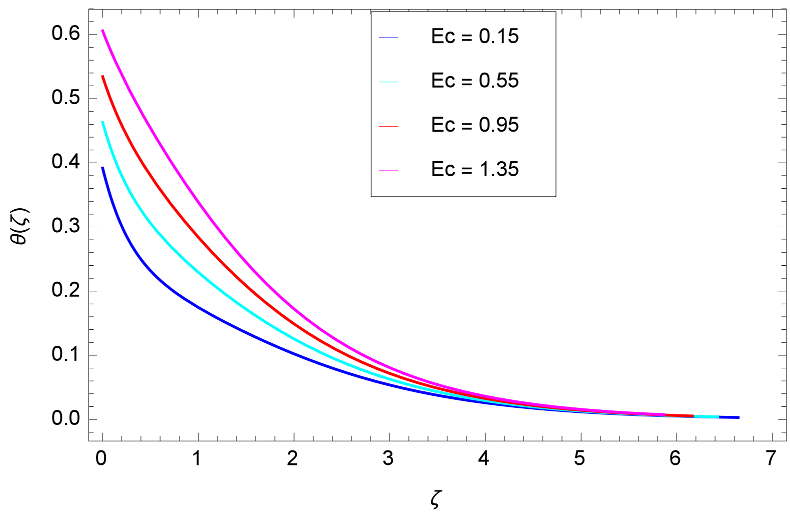

Figure 15. Influence of Ec on $\theta(\zeta)$.

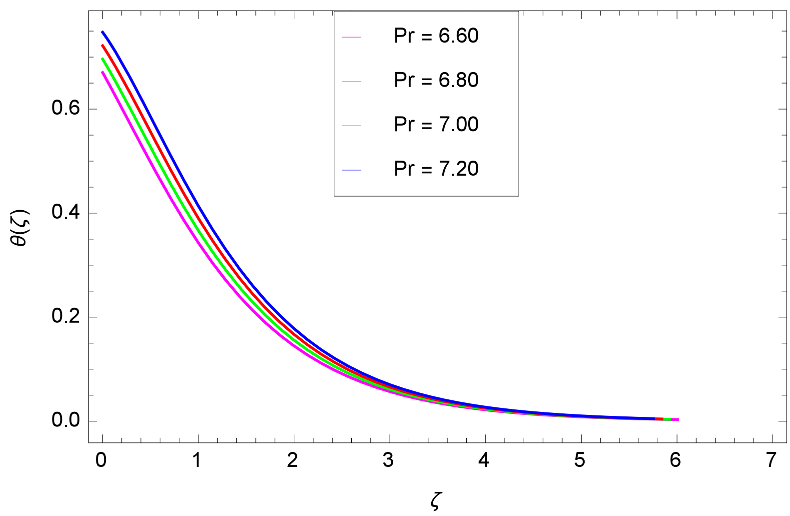

Figure 16. Influence of Pr on $\theta(\zeta)$.

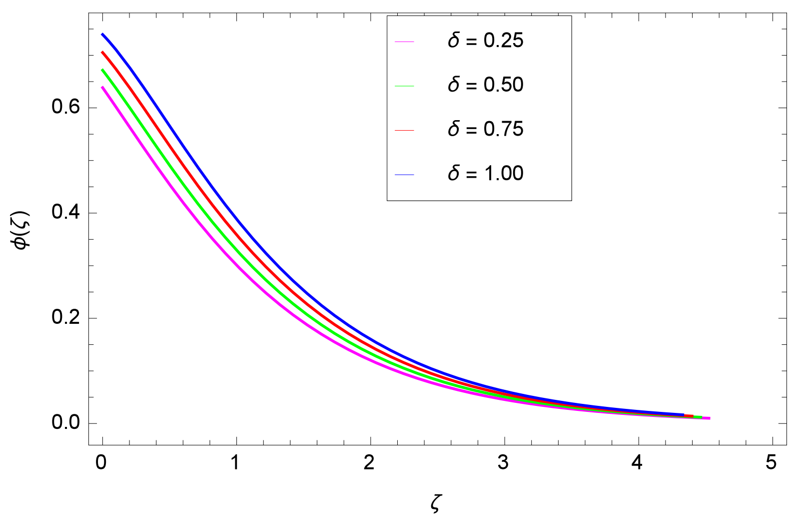

Figure 17. Influence of δ on $\phi(\zeta)$.

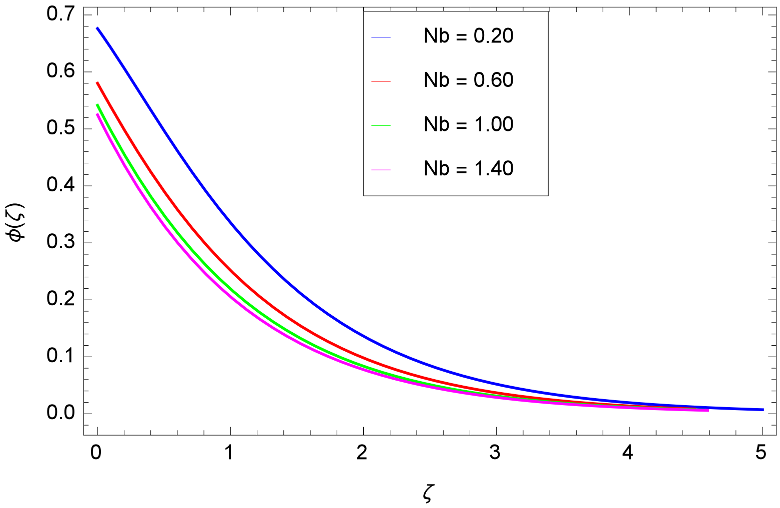

Figure 18. Influence of Nb on $\phi(\zeta)$.

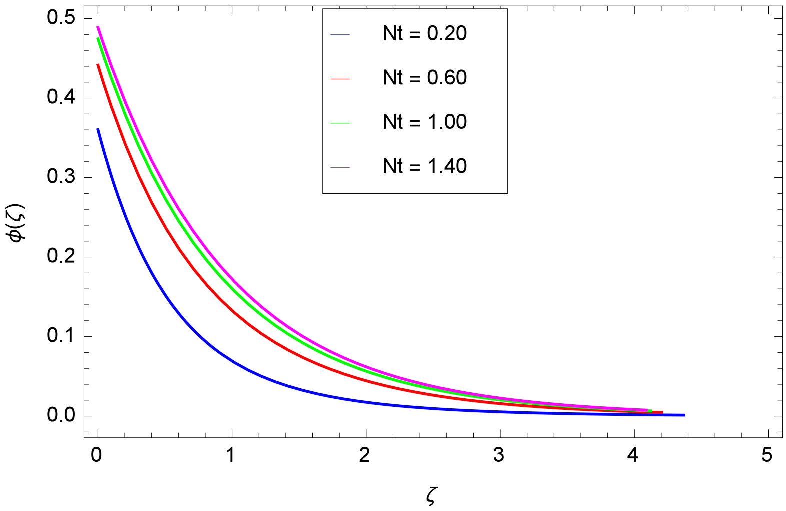

Figure 19. Influence of Nt on $\phi(\zeta)$.

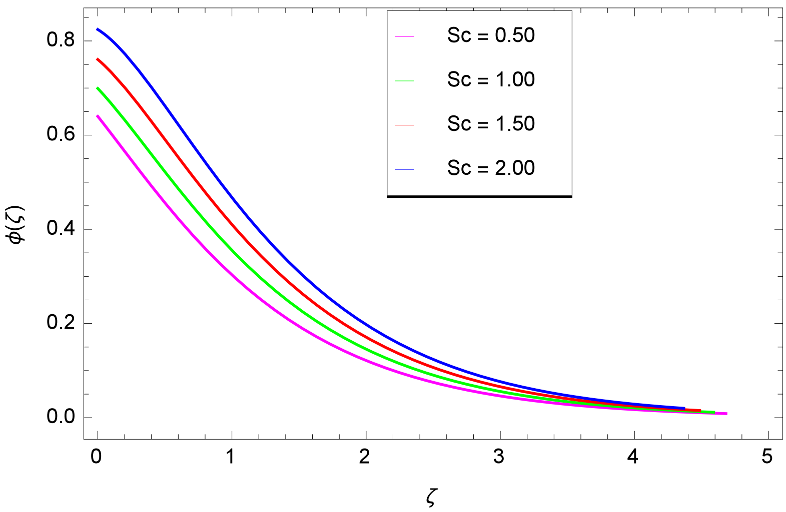

Figure 20. Influence of Sc on $\phi(\zeta)$.

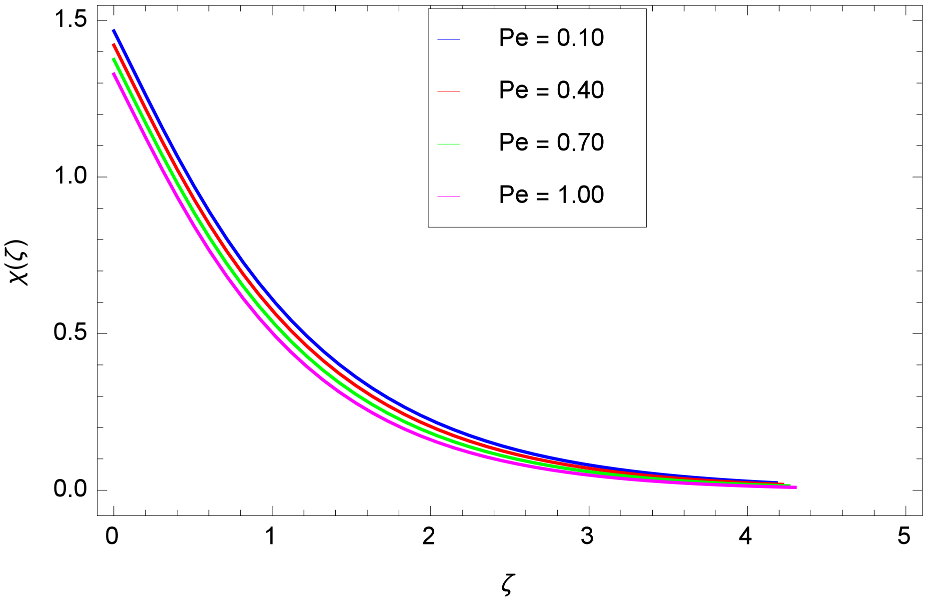

Figure 21. Influence of Pe on $\chi(\zeta)$.

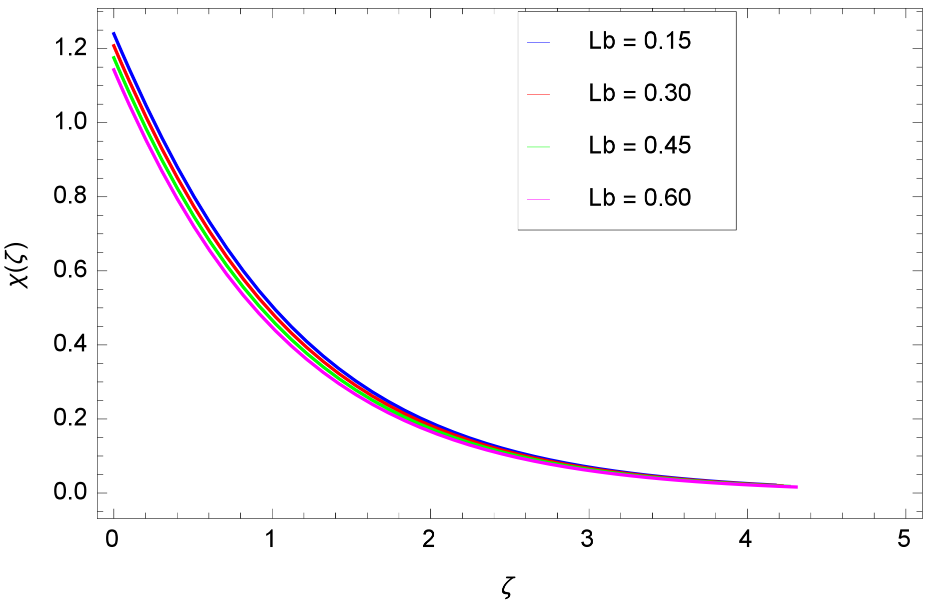

Figure 22. Influence of Lb on $\chi(\zeta)$.

Table 3. Influence of $\beta,\ \varepsilon,\ \lambda,\ S,\ Rd,\ Fr,\ Ec,$ and Pr on $\theta'(0)$.

β	ε	λ	S	Rd	Fr	Ec	Pr	$\theta'(0)$
0.2	0.3	0.2	0.4	0.3	0.2	0.1	0.7	0.44701
0.3								0.43167
0.5								0.40752
	0.4							0.39766
	0.5							0.38914
	0.6							0.37245
		0.5						0.45806
		0.8						0.45739
		1.1						0.45623
			0.8					1.03123
			1.2					0.87433
			1.6					0.64876
				0.5				0.45342
				0.7				0.44534
				0.9				0.43998
					0.6			0.64554
					1.0			0.63854
					1.4			0.61291
						0.3		0.38453
						0.5		0.38123
						0.7		0.37941
							6.7	0.75651
							7.7	0.80612
							8.7	0.86432

Table 4. Influence of $\delta,\ Sc,\ Nb$ on $\phi'(0)$.

δ	Sc	Nb	$\phi'(0)$
0.2	0.3	0.5	1.28733
0.4			1.26931
0.6			1.24887
	0.5		1.32742
	0.7		1.31022
	0.9		1.30271
		1.0	1.33075
		1.5	1.41186
		2.0	1.47572

Table 5. Influence of $N_\delta,\ Pe,\ Lb,\ Ra_b$ on $\chi'(0)$.

δ_n	Pe	Lb	Ra_b	$\chi'(0)$
0.1	0.3	0.3	0.2	0.57238
0.2				0.56103
0.3				0.55271
	0.5			0.42714
	1			0.45102
	1.5			0.49327
		0.5		0.53185
		1		0.62386
		1.5		0.66671
			0.3	0.75408
			0.4	0.76965
			0.5	0.77121

6. Conclusions

A vertical cone has been used to study the flow of ferromagnetic nanofluid with bioconvection and magnetic dipole elements. There is also evidence of the Darcy–Forchheimer flow model. Viscosity dissipation, Brownian motion, chemical reaction, and thermophoresis are involved. Using appropriate transformations, nonlinear PDEs were reduced to a set of nonlinear ODEs. The important outcomes are listed below:

- The velocity decreases as the ferromagnetic interaction parameter, porosity parameter, and local inertia parameter increase.
- The temperature rises as the ferromagnetic interaction, heat dissipation, injection, thermal radiation parameters and Eckert number are raised, and reduces when the Prandtl number and sunction parameter are raised.
- When the Brownian motion, chemical reaction parameters and Schmidt number increase, the concentration decreases, while it increases when the thermophoresis parameter increases.
- The motile microorganism density decreases through raising the Peclet number and bioconvection Lewis number.

Author Contributions: A.H.U. and W.K. formulated and solved the problem. A.H.U. and Z.S. wrote the draft and the revised manuscript. A.H.U. and Z.S. sketched the graphs. U.W.H. and P.K. performed the investigations, supervision, and funding. All authors have read and agreed to the published version of the manuscript.

Funding: This research received no external funding.

Institutional Review Board Statement: Not applicable.

Informed Consent Statement: Not applicable.

Data Availability Statement: Availability exists for entirety of the data.

Acknowledgments: This research project is supported by Thailand Science Research and Innovation (TSRI) Basic Research Fund: Fiscal year 2022. The authors are thankful to KMUTT for providing the technical and financial support. The first author is supported by the Petchra Pra Jom Klao Doctoral Scholarship Academic for Ph.D. program of King Mongkut's University of Technology Thonburi (KMUTT) [Grant No. 13/2562].

Conflicts of Interest: The authors have no conflict of interests.

References

1. Raj, K.; Moskowitz, R. Commercial applications of ferrofluids. *J. Magn. Magn. Mater.* **1990**, *85*, 233–245. [CrossRef]
2. Goldman, A. *Handbook of Modern Ferromagnetic Materials*; Springer Science and Business Media: Berlin, Germany, 2012.
3. Hathway, D.B. dB-sound. *Eng. Mag.* **1979**, *13*, 42–44.
4. Andersson, H.I.; Valnes, O.A. Flow of a heated ferrofluid over a stretching sheet in the presence of a magnetic dipole. *Acta Mech.* **1998**, *128*, 39–47. [CrossRef]
5. Zeeshan, A.; Majeed, A.; Ellahi, R.; Zia, Q.M.Z. Mixed convection flow and heat transfer in ferromagnetic fluid over a stretching sheet with partial slip effects. *Therm. Sci.* **2018**, *22*, 2515–2526. [CrossRef]
6. Hayat, T.; Ahmad, S.; Khan, M.I.; Alsaedi, A. Exploring magnetic dipole contribution on radiative flow of ferromagnetic Williamson fluid. *Results Phys.* **2018**, *8*, 545–551. [CrossRef]
7. Choi, S.U.; Eastman, J.A. *Enhancing Thermal Conductivity of Fluids with Nanoparticles*; Argonne National Lab: Lemont, IL, USA, 1995.
8. Ellahi, R. The effects of MHD and temperature dependent viscosity on the flow of non-Newtonian nanofluid in a pipe: Analytical solutions. *Appl. Math. Model.* **2013**, *37*, 1451–1467. [CrossRef]
9. Ellahi, R.; Raza, M.; Akbar, N.S. Study of peristaltic flow of nanofluid with entropy generation in a porous medium. *J. Porous Media* **2017**, 20, 461–478. [CrossRef]
10. Hayat, T.; Ahmad, S.; Khan, M.I.; Alsaedi, A. Modeling and analyzing flow of third grade nanofluid due to rotating stretchable disk with chemical reaction and heat source. *Phys. B Condens. Matter.* **2018**, *537*, 116–126. [CrossRef]
11. Awais, M.; Shah, Z.; Perveen, N.; Ali, A.; Kumam, P.; Thounthong, P. MHD effects on ciliary-induced peristaltic flow coatings with rheological hybrid nanofluid. *Coatings* **2020**, *10*, 186. [CrossRef]

12. Reddy, P.S.; Sreedevi, P.; Chamkha, A.J. MHD natural convection boundary layer flow of nanofluid over a vertical cone with chemical reaction and suction/injection. *Comput. Therm. Sci. Int. J.* **2017**, 9, 165–182. [CrossRef]
13. Alsaedi, A.; Khan, M.I.; Farooq, M.; Gull, N.; Hayat, T. Magnetohydrodynamic (MHD) stratified bioconvective flow of nanofluid due to gyrotactic microorganisms. *Adv. Powder Technol.* **2017**, *28*, 288–298. [CrossRef]
14. Hayat, T.; Bashir, Z.; Qayyum, S.; Alsaedi, A. Nonlinear radiative flow of nanofluid in presence of gyrotactic microorganisms and magnetohydrodynamic. *Int. J. Numer. Methods Heat Fluid Flow* **2019**, *29*, 3039–3055. [CrossRef]
15. Nadeem, S.; Ijaz, M.; El-Kott, A.; Ayub, M. Rosseland analysis for ferromagnetic fluid in presence of gyrotactic microorganisms and magnetic dipole. *Ain Shams Eng. J.* **2020**, *11*, 1295–1308. [CrossRef]
16. Bhatti, M.M.; Michaelides, E.E. Study of Arrhenius activation energy on the thermo-bioconvection nanofluid flow over a Riga plate. *J. Therm. Anal. Calorim.* **2021**, *143*, 2029–2038. [CrossRef]
17. Waqas, H.; Khan, S.A.; Alghamdi, M.; Alqarni, M.S.; Muhammad, T. Numerical simulation for bio-convection flow of magnetized non-Newtonian nanofluid due to stretching cylinder/plate with swimming motile microorganisms. *Eur. Phys. J. Spec. Top.* **2021**, *230*, 1239–1256. [CrossRef]
18. Ingham, D.B.; Pop, I. (Eds.) *Transport Phenomena in Porous Media III*; Elsevier: Oxford, UK, 2005; Volume 3.
19. Zeng, Z.; Grigg, R. A criterion for non-Darcy flow in porous media. *Transp. Porous Media* **2006**, *63*, 57–69. [CrossRef]
20. Kumar, B.R.; Sivaraj, R. MHD viscoelastic fluid non-Darcy flow over a vertical cone and a flat plate. *Int. Commun. Heat Mass Transf.* **2013**, *40*, 1–6. [CrossRef]
21. Chamkha, A.; Abbasbandy, S.; Rashad, A.M. Non-Darcy natural convection flow for non-Newtonian nanofluid over cone saturated in porous medium with uniform heat and volume fraction fluxes. *Int. J. Numer. Method Heat Fluid Flow* **2015**, *25*, 422–437. [CrossRef]
22. Mallikarjuna, B.; Rashad, A.M.; Hussein, A.K.; Raju, S.H. Transpiration and thermophoresis effects on Non-Darcy convective flow past a rotating cone with thermal radiation. *Arab. J. Sci. Eng.* **2016**, *41*, 4691–4700. [CrossRef]
23. Durairaj, M.; Ramachandran, S.; Mehdi, R.M. Heat generating/absorbing and chemically reacting Casson fluid flow over a vertical cone and flat plate saturated with non-Darcy porous medium. *Int. J. Numer. Method Heat Fluid Flow* **2017**, *27*, 156–173. [CrossRef]
24. Pătrulescu, F.O.; Groşan, T.; Pop, I. Natural convection from a vertical plate embedded in a non-Darcy bidisperse porous medium. *J. Heat Transf.* **2020**, 142, 012504. [CrossRef]
25. Liao, S.J. The Proposed Homotopy Analysis Method for the Solution of Nonlinear Problems. Ph.D. Thesis, Shanghai Jiao Tong University, Shanghai, China, 1992.
26. Liao, S.J. An explicit, totally analytic approximate solution for Blasius viscous flow problems. *Int. J. Non-Linear Mech.* **1999**, *34*, 759–778. [CrossRef]
27. Liao, S. *Beyond Perturbation: Introduction to the Homotopy Analysis Method*; CRC Press: Boca Raton, FL, USA, 2003.
28. Irfan, M.; Khan, M.; Khan, W.A.; Sajid, M. Thermal and solutal stratifications in flow of Oldroyd-B nanofluid with variable conductivity. *Appl. Phys. A* **2018**, *124*, 674. [CrossRef]
29. Tlili, I.; Waqas, H.; Almaneea, A.; Khan, S.U.; Imran, M. Activation energy and second order slip in bioconvection of Oldroyd-B nanofluid over a stretching cylinder: A proposed mathematical model. *Processes* **2019**, *7*, 914. [CrossRef]
30. Usman, A.H.; Khan, N.S.; Humphries, U.W.; Ullah, Z.; Shah, Q.; Kumam, P.; Thounthong, P.; Khan, W.; Kaewkhao, A.; Bhaumik, A. Computational optimization for the deposition of bioconvection thin Oldroyd-B nanofluid with entropy generation. *Sci. Rep.* **2021**, *11*, 11641. [CrossRef] [PubMed]
31. Hayat, T.; Waqas, M.; Shehzad, S.A.; Alsaedi, A. Mixed convection flow of viscoelastic nanofluid by a cylinder with variable thermal conductivity and heat source/sink. *Int. J. Numer. Method Heat Fluid Flow* **2016**, *26*, 214–234. [CrossRef]